



Multimodal cotranslational interactions direct assembly of the human multi-tRNA synthetase complex

Krishnendu Khan^a, Briana Long^a, Valentin Gogonea^b, Gauravi M. Deshpande^c, Kommireddy Vasu^a, and Paul L. Fox^{a,b,1}

Edited by Michael Ibba, Chapman University, Orange, CA; received March 31, 2022; accepted August 4, 2022 by Editorial Board Member Robert S. Langer

Amino acid ligation to cognate transfer RNAs (tRNAs) is catalyzed by aminoacyl-tRNA synthetases (aaRSs)—essential interpreters of the genetic code during translation. Mammalian cells harbor 20 cytoplasmic aaRSs, out of which 9 (in 8 proteins), with 3 non-aaRS proteins, AIMP1 to 3, form the ~1.25-MDa multi-tRNA synthetase complex (MSC). The function of MSC remains uncertain, as does its mechanism of assembly. Constituents of multiprotein complexes encounter obstacles during assembly, including inappropriate interactions, topological constraints, premature degradation of unassembled subunits, and suboptimal stoichiometry. To facilitate orderly and efficient complex formation, some complexes are assembled cotranslationally by a mechanism in which a fully formed, mature protein binds a nascent partner as it emerges from the translating ribosome. Here, we show out of the 121 possible interaction events between the 11 MSC constituents, 15 are cotranslational. AIMP1s are involved in the majority of these cotranslational interactions, suggesting they are not only critical for MSC structure but also for assembly. Unexpectedly, several cotranslational events involve more than the usual dyad of interacting proteins. We show two modes of cotranslational interaction, namely a “multisite” mechanism in which two or more mature proteins bind the same nascent peptide at distinct sites and a second “piggy-back” mechanism in which a mature protein carries a second fully formed protein and binds to a single site on an emerging peptide. Multimodal mechanisms of cotranslational interaction offer a diversity of pathways for ordered, piecewise assembly of small subcomplexes into larger heteromultimeric complexes such as the mammalian MSC.

multi-tRNA synthetase complex | aminoacyl-tRNA synthetase | cotranslational interaction | multiprotein complex | complex assembly

The mammalian proteome comprises an array of protein complexes, generally with well-defined stoichiometries, that participate in nearly all cellular activities including transport, signal transduction, maintenance of structural integrity, and metabolism, among others (1–3). The complexes can be homomultimeric, as in the case of some cytoskeletal structures, or heteromultimeric. The latter can contain repeats of a small group of proteins, such as the proteasome, or can consist of a completely heterogeneous population, such as both ribosomal subunits (that also contain rRNA) (4, 5). The assembly of multiprotein complexes can be constitutive or stimulus-dependent; the latter generally depends on protein phosphorylation and other posttranslational modifications (6). Unlike the role of polycistronic operons in complex assembly in prokaryotes, in eukaryotes the genes encoding functionally related proteins are scattered among chromosomes (7, 8). It is generally considered that multiprotein complexes are assembled by stochastic or chaperone-instructed, domain-specific interactions between fully formed, mature constituents (“posttranslational assembly”). However, assembly of several complexes recently has been shown to employ a distinct “cotranslational” mechanism in which a mature, fully formed constituent interacts with a nascent peptide of the partner constituent as it emerges from the ribosome traversing the encoding messenger RNA (mRNA) (Fig. 1*A*, *Left*) (9, 10). Cotranslational assembly offers multiple advantages, including shielding of a constituent that in free form is susceptible to aggregation or degradation or is deleterious to cell health (9–12). Also, the mechanism can facilitate formation of interactions between proteins in which a binding domain is masked or otherwise inaccessible in one of the mature partners (13). Protein folding during de novo synthesis is facilitated by chaperones that bind nascent protein and reduce nonspecific hydrophobic interactions; likewise, a similar role for chaperones has been proposed to facilitate cotranslational complex assembly, but experimental evidence is lacking (11). Recent investigations of complex assembly in yeast revealed the process is pervasive, with 12 out of 31 and 9 out of 12 complexes assembled cotranslationally (10, 11). An important role of cotranslational complex assembly in the mammalian proteome is currently emerging (12, 14).

Significance

Multiprotein complexes form by stochastic interactions between mature proteins or by chaperone-facilitated interactions. Certain complexes form by a cotranslational mechanism in which a fully folded protein binds the N terminus of its partner emerging from the translating ribosome. The multi-tRNA (transfer RNA) synthetase complex (MSC) is among the largest heteromultimeric complexes, containing 11 distinct proteins. We show cotranslational interactions contribute to assembly of several MSC subcomplexes by novel cotranslational mechanisms, i.e., a “multisite” mechanism in which multiple proteins bind the same emerging peptide at distinct sites and a “piggy-back” mechanism in which a mature protein carries a second protein to the emerging peptide. This work will be interesting to investigators of aminoacyl-tRNA synthetases, multiprotein complexes, and complex assembly, among others.

Author contributions: K.K. and P.L.F. designed research; K.K., B.L., V.G., and K.V. performed research; K.K., V.G., G.M.D., and P.L.F. analyzed data; and K.K. and P.L.F. wrote the paper.

The authors declare no competing interest.

This article is a PNAS Direct Submission. M.I. is a guest editor invited by the Editorial Board.

Copyright © 2022 the Author(s). Published by PNAS. This article is distributed under Creative Commons Attribution-NonCommercial-NoDerivatives License 4.0 (CC BY-NC-ND).

¹To whom correspondence may be addressed. Email: foxp@ccf.org.

This article contains supporting information online at <http://www.pnas.org/lookup/suppl/doi:10.1073/pnas.2205669119/-DCSupplemental>.

Published August 29, 2022.

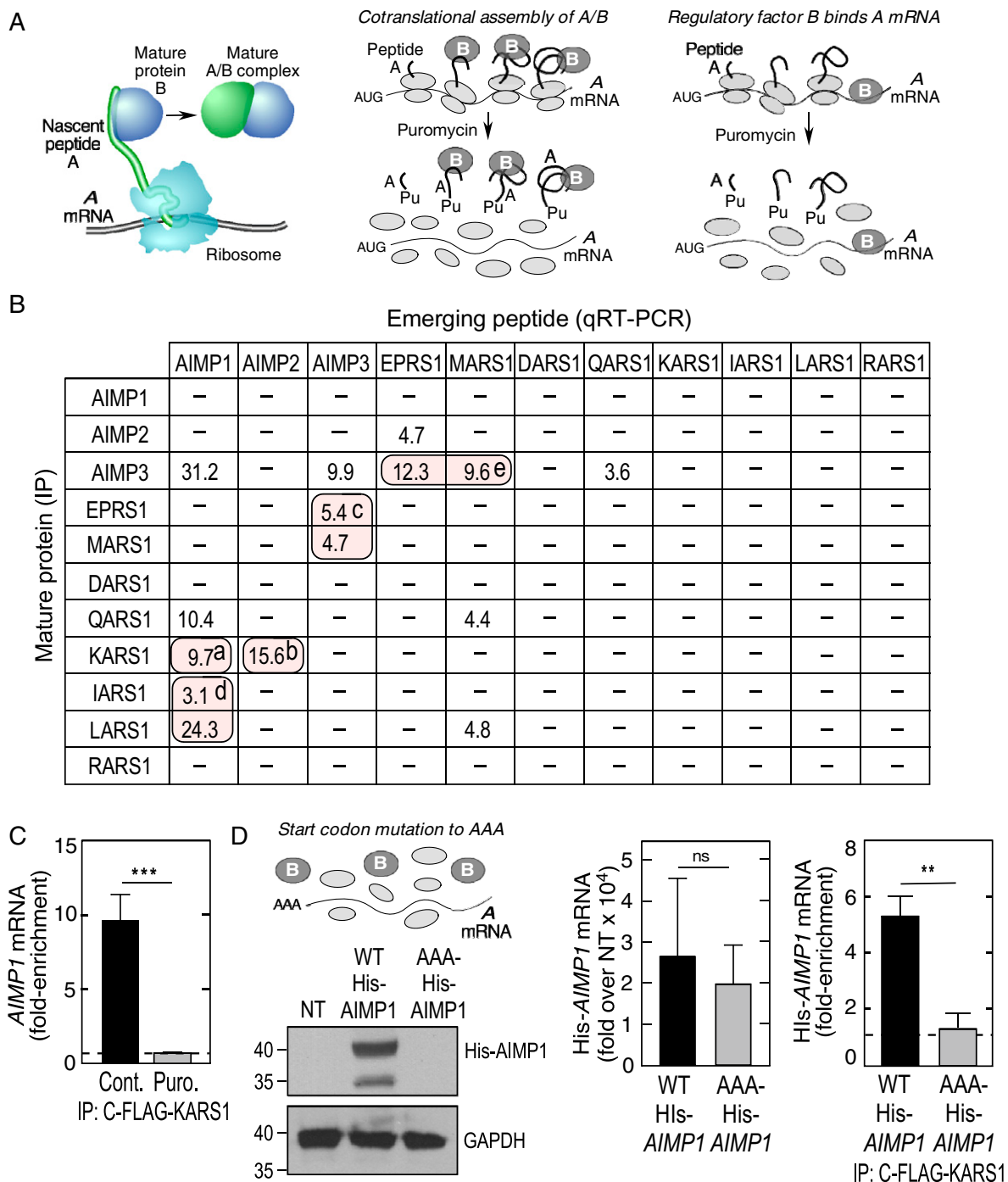


Fig. 1. Cotranslational interaction of select MSC constituents. (A) Schematic of cotranslational interaction between proteins (*Left*). Cotranslational interaction between mature protein with nascent, translating partner mRNA is puromycin-sensitive (*Center*). Interaction between regulatory RNA-binding protein and target mRNA is puromycin-resistant (*Right*). (B) Matrix of cotranslational interactions between MSC constituents. HEK293T cells were transfected with C-FLAG-tagged, full-length MSC constituents, incubated with or without puromycin (Puro.) and lysates subjected to RIP with IgG or anti-FLAG antibodies followed by qRT-PCR with constituent-specific probes. The rows correspond to the mature FLAG-tagged MSC proteins, and columns correspond to mRNAs of nascent target proteins. Shown is fold enrichment of mRNA following pulldown with constituent-specific antibody compared to isotype-specific IgG, as determined by RIP-qRT-PCR (mean, $n = 3$). “-” indicates no enrichment or fold enrichment less than 3.0. Superscript a indicates the cotranslational interaction between KARS1 and AIMP1, b the cotranslational interaction between KARS1 and AIMP2, c the cotranslational interaction between EPRS1 and MARS1 with AIMP3, d the cotranslational interaction between IARS1 and LARS1 with AIMP1, and e the cotranslational interaction between AIMP3 with EPRS1 and MARS1. (C) KARS1 and AIMP1 interact cotranslationally. HEK293T cells were transfected with C-FLAG-KARS1 construct and incubated in the absence or presence of puromycin. Lysates were subjected to RIP with IgG or anti-FLAG antibodies followed by qRT-PCR with *AIMP1* mRNA probe. mRNA is expressed as fold enrichment compared to isotype-specific IgG RIP-qRT-PCR. Mean + SD, $n = 3$; $***P < 0.001$. (D) Translation is required for KARS1-AIMP1 interaction. Schematic of experiment with ATG-to-AAA mutant (*Top Left*). HEK293T cells were transfected with wild-type (WT) or ATG-to-AAA start codon mutant His-AIMP1 construct and lysates probed with anti-His and -GAPDH antibodies (*Bottom Left*) and His-AIMP1 mRNA expression determined by qRT-PCR and compared to nontransfected (NT) control (*Center*). Cells were cotransfected with C-FLAG-KARS1 and WT or ATG-to-AAA mutated His-AIMP1 constructs and lysates subjected to anti-FLAG RIP-qRT-PCR with *His-AIMP1* mRNA probe. mRNA is expressed as fold enrichment compared to isotype-specific IgG RIP-qRT-PCR (*Right*). Mean + SD, $n = 3$; $**P < 0.01$; ns = nonsignificant.

Among the very large mammalian heteromultimeric complexes is the ~1.25-MDa multi-tRNA (transfer RNA) synthetase complex (MSC). Cells contain 20 aminoacyl-tRNA synthetases (aaRSs), 1 for each of the 20 amino acids (15). The canonical function of aaRSs is the ligation of amino acids to their cognate tRNAs for accurate interpretation of the genetic code during mRNA translation. During evolution, beginning in archaea, relatively small MSC structures were formed by interactions between several specific aaRSs and auxiliary scaffolding proteins (16). The yeast MSC, a ternary structure containing EARS1, MARS1, and the structural protein Arc1, is thought to be an evolutionary intermediate between the earliest structures and the megacomplex in higher eukaryotes (17). (Nomenclature: for human aaRSs, the one-letter amino acid code is used, followed by ARS1, where 1 signifies a nucleus-encoded gene; for clarity the same convention is used here for yeast proteins.) The mammalian MSC contains nine aaRS activities (in eight polypeptides as EPRS1 is a bifunctional aaRS in which EARS1 and PARS1 are covalently linked) and three nonsynthetase proteins, AIMP3 1, 2, and 3, considered to be primarily structural. AIMP3 is a functional homolog of yeast Arc1, but Arc1 shares sequence homology with AIMP1 (18). The function of the mammalian MSC remains uncertain. MSC binding to ribosomes has been proposed to facilitate “channeling” of charged tRNAs into the ribosome A-site for improved translation efficiency (19–23). However, translation is not affected when the majority of EPRS1, or all RARS1 and QARS1, are excluded from the MSC, providing evidence against a significant MSC role in global protein synthesis (24, 25). Alternatively, the MSC can act as a “depot” that sequesters constituents, thereby preventing injurious ectopic, extra-MSC activities, while permitting condition- and stimulus-dependent release of aaRSs to perform noncanonical functions unrelated to their principal roles in protein synthesis (26). This hypothesis has been supported by reports of stimulus-dependent MSC release of EPRS1 (24, 27), KARS1 (28), MARS1 (29), and AIMP3 (30). Release is triggered by posttranslational modification of the released constituent, generally phosphorylation (27, 28, 31, 32).

The structures of nearly all individual MSC constituents have been resolved by X-ray crystallography, as well as the structures of several subcomplexes (33–36). Many of the intermolecular interactions involve relatively small noncatalytic domains, appended during evolution (37–39). A three-dimensional architecture of the human MSC has been described that combines high-resolution structural data with proximity information derived from cross-linking mass spectrometry (XL-MS) (40, 41). The structure is relatively compact, with substantial clefts and lacking apparent symmetry. All constituents are surface-exposed, facilitating interaction with charged tRNA substrates. In view of their inducible, extra-MSC functions, it is likely that the conformation of constituents in the MSC permits interaction with regulatory proteins, e.g. kinases. Although structural and functional aspects of the MSC have been investigated extensively, its mechanism of assembly remains essentially unexplored. One possibility is a chaperone-mediated assembly as in the case of the ribosomal subunits that require more than 200 protein assembly factors (42). Alternatively, assembly might take advantage of cotranslational interactions (which might also utilize chaperones). The second mechanism is supported by experiments in yeast that show the ternary MSC is assembled by multiple cotranslational interactions between the constituents (11). Here, we have systematically determined the cotranslational landscape of the human MSC. By a series of RNA immunoprecipitation (RIP) assays followed by qRT-PCR, we show several known multiprotein MSC subcomplexes are assembled cotranslationally. Notably, several

cotranslational interactions occur by coordination mechanisms not previously described.

Results

Cotranslational Landscape of the Human MSC. Direct determination of the cotranslational interaction of a mature protein with a nascent peptide is hindered by the technical difficulty of capturing the peptide during its limited lifetime before maturation. Moreover, the relatively low amount of the interacting complex in the short-lived transition state requires a high-sensitivity assay. To overcome these obstacles, a proxy assay is generally used to score cotranslational interaction by determining binding of the mature protein to the ribosome-bound mRNA encoding the nascent peptide during translation (Fig. 1*A*, *Left*). The cotranslational interaction is thus identified by RIP of the mature protein, followed by highly sensitive qRT-PCR (or RNA sequencing) to detect the enriched mRNA encoding the nascent protein. To differentiate between cotranslational and posttranslational RNA–protein interaction, for example in the case of regulatory RNA-binding proteins, parallel experiments are done in the presence of puromycin to disassemble the translation machinery. Puromycin-independent binding of the mature protein to the mRNA indicates cotranslational interaction (Fig. 1*A*, *Center*); continued interaction in the presence of puromycin suggests binding of a regulatory factor (Fig. 1*A*, *Right*). To investigate the potential role of cotranslation in assembly of the human MSC, C-terminal FLAG-tagged complementary DNA (cDNA) constructs expressing all 11 full-length MSC constituents were transfected individually in HEK293T cells in the presence or absence of puromycin. The full-length expressed proteins were immunoprecipitated from cell lysates with monoclonal anti-FLAG antibodies or normal mouse immunoglobulin G (IgG) control, followed by qRT-PCR using primers specific for each MSC component. A stringent cutoff of at least threefold, puromycin-independent target mRNA enrichment by FLAG antibody pull-down compared to IgG pull-down was used to establish cotranslational interaction. Out of 121 potential interactions, 15 were found to be cotranslational (Fig. 1*B* and [Dataset S1](#)). All but two of these interactions between MSC constituents involved the three AIMP3s, either as the mature or nascent target protein, consistent with the generally accepted concept that they are nonenzymatic, structural constituents of the MSC.

The cotranslational interaction of KARS1 with nascent AIMP1 (Fig. 1*B*, superscript a) was investigated in more detail since only a weak binary interaction between these constituents has been described (43). Overexpression, followed by pull-down of C-FLAG-KARS1 with anti-FLAG antibody, caused a 9.7-fold enrichment in *AIMP1* mRNA, and the interaction was completely disrupted by puromycin, supporting a cotranslational mechanism (Fig. 1*C*). To validate the cotranslational interaction, the requirement for translation was probed. A C-His-tagged *AIMP1* cDNA construct was generated in which the ATG start codon was mutated to AAA, previously shown to prevent cotranslational interaction (Fig. 1*D*, *Top Left*) (10). ATG-to-AAA mutation of the initiation codon of the *AIMP1* construct abrogated protein expression, as expected; the lower band is likely a degradation product of AIMP1 as it is also inhibited by start codon mutation (Fig. 1*D*, *Bottom Left*). As a transfection efficiency control, both constructs were shown to be equally expressed (Fig. 1*D*, *Center*). C-FLAG-KARS1 was coexpressed with either wild-type or mutant His-*AIMP1* cDNAs and subjected to RIP with anti-FLAG antibody followed by qRT-PCR. Robust enrichment

of wild-type, but not mutant, *AIMP1* mRNA was observed, validating the requirement for translation (Fig. 1D, Right).

Cotranslational Interaction of KARS1 and AIMP2. We investigated in detail the cotranslational binding of mature KARS1 with AIMP2 peptide (Fig. 1B, superscript b), an interaction structurally determined by X-ray crystallography and further characterized by XL-MS (Fig. 2A and SI Appendix, Fig. S1) (36, 40). FLAG pull-down of C-FLAG-KARS1, followed by RIP-qRT-PCR, revealed marked *AIMP2* mRNA enrichment; near-complete reversal by puromycin treatment of HEK293T cell lysates supported a cotranslational mechanism (Fig. 2B). Peptide epitope mimetics (PEM) mimicking the N terminus of nascent proteins can abrogate cotranslational events (13). Moreover, the N-terminal 36 amino acids of AIMP2 are critical for its interaction with KARS1 (Fig. 2A and SI Appendix, Fig. S1) (36, 40). A PEM corresponding to the N-terminal 36 amino acids of AIMP2 bearing an upstream 9-Arg sequence (Arg₉-AIMP2) to promote membrane permeation was synthesized, as well as a scrambled control PEM (Arg₉-scrambled). HEK293T cells overexpressing C-FLAG KARS1 were incubated with the Arg₉-containing peptides, followed by RIP with anti-FLAG antibody and qRT-PCR. Arg₉-AIMP2 treatment markedly reduced the enrichment of *AIMP2* mRNA, consistent with abrogation of cotranslational interaction (Fig. 2C).

To investigate the consequences of disturbing KARS1/AIMP2 interaction, stable HEK293T lines were generated in which KARS1 and AIMP2 separately were subjected to short hairpin RNA (shRNA)-mediated knockdown (KD) (Fig. 2D,

Top). To determine the effect of KD on MSC retention, cell lysates from shControl (shCtrl), shKARS1, and shAIMP2 KD cells were subjected to size-exclusion chromatography. In shCtrl cells, KARS1 and AIMP2 elute in high-molecular-weight fractions consistent with primary residence in the MSC (Fig. 2D, Bottom). However, AIMP2 KD caused a shift of a substantial amount of KARS1 to lower-molecular-weight fractions consistent with a free KARS1 dimer. KARS1 KD did not substantially alter MSC retention of AIMP2. These results suggest interaction with AIMP2, a known structural protein, is critical for incorporation of KARS1 in the MSC, but not the converse. A fraction of KARS1 in the shCtrl KD elutes in a region outside the MSC but greater than ~0.5 MDa, consistent with an MSC subcomplex or an undefined complex. Nuclear localization of KARS1 has been reported (44, 45), and a small amount of extra-MSC KARS1 translocates to the nucleus in AIMP2 KD cells as shown by immunofluorescence (Fig. 2E).

Multiprotein, Cotranslational Interaction of EPRS1, MARS1, and AIMP3.

The observation that both mature EPRS1 and MARS1 bind nascent AIMP3 (Fig. 1B, superscript c) raises important mechanistic questions on how two (or more) mature proteins bind the same nascent protein, and several pathways are possible (Fig. 3). In “multisite” cotranslation, two or more mature proteins bind distinct sites on the nascent peptide. “Concurrent” multisite binding of two mature proteins to nascent peptide would lead directly to ternary complex formation (Fig. 3A, Left). In an alternative “serial” mechanism, a single mature protein binds the nascent peptide to form a binary complex, possibly

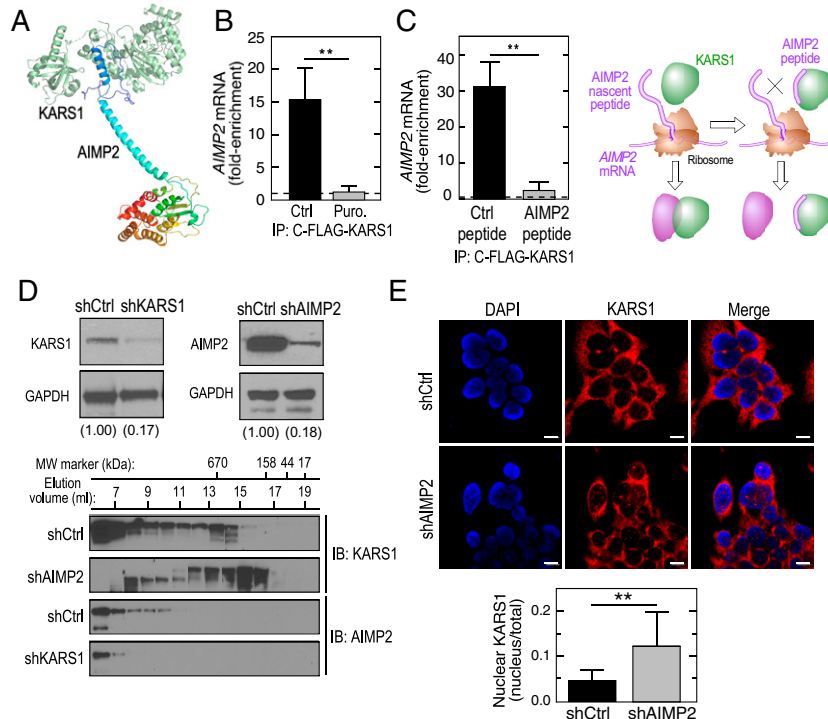


Fig. 2. Cotranslational interaction between KARS1 and AIMP2. (A) XL-MS-based structure showing KARS1 interacts with the AIMP2 N terminus (Left). (B) Cotranslational interaction of KARS1 and AIMP2. HEK293T cells were transfected with C-FLAG-KARS1 construct, incubated in the absence and presence of puromycin, and lysates subjected to RIP with IgG or anti-FLAG antibodies followed by qRT-PCR with *AIMP2* mRNA probe. mRNA is expressed as fold enrichment compared to isotype-specific IgG RIP-qRT-PCR. Mean + SD, $n = 3$; $**P < 0.01$. (C) PEM of AIMP2 N terminus abrogates cotranslational interaction of KARS1 with AIMP2. HEK293T cells were transfected with C-FLAG-tagged KARS1, treated with Arg₉-AIMP2 or scrambled peptides, and subjected to RIP with IgG or anti-FLAG antibodies followed by qRT-PCR with *AIMP2* mRNA probe (Left). mRNA is expressed as fold enrichment compared to isotype-specific IgG RIP-qRT-PCR. Mean + SD, $n = 3$; $**P < 0.01$. Schematic depicting inhibitory activity of AIMP2 mimetic peptide (Right). (D) AIMP2 influences KARS1 inclusion in the MSC. shCtrl and shKARS1 cells were subjected to immunoblot with anti-KARS1 and anti-GAPDH antibodies (Top Left). shCtrl and shAIMP2 cells were subjected to immunoblot with anti-AIMP2 and anti-GAPDH antibodies (Top Right). shCtrl, shAIMP2, and shKARS1 cell lysates were subjected to gel filtration chromatography followed by immunoblot with anti-KARS1 and anti-AIMP2 antibodies. (E) Immunofluorescence analysis of shCtrl and shAIMP2 cells using anti-KARS1 antibody and DAPI (Top). (Scale bars, 10 μ m.) Bar plots report the nuclear enrichment of KARS1 under different conditions; mean + SD, $**P < 0.01$ (Bottom).

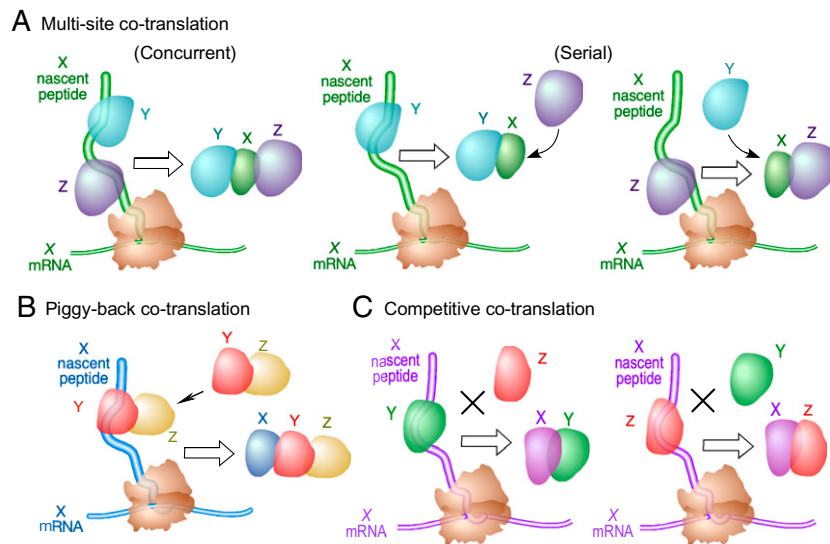


Fig. 3. Schematics of multiple modes of cotranslation. (A) Multisite cotranslation can occur by two pathways. In the “concurrent” mechanism, two mature proteins, Y and Z, bind at the same time to the N terminus of their common binding partner X at distinct sites, resulting in formation of a ternary complex where both Y and Z are directly associated with X (Left). In the “serial” mechanism, a single mature protein binds nascent peptide to form a binary complex, possibly followed by binding of a second mature protein to form a ternary complex (right two panels) (B) Piggy-back cotranslation. Two mature proteins, Y and Z, form a dimeric complex that binds to the N terminus of X via Y, resulting in formation of ternary complex where Z is indirectly associated with X. (C) Competitive cotranslation. Two mature proteins, Y and Z, bind the same site in the N terminus of a common binding partner, X, resulting in competitive inhibition of binding, potentially resulting in two distinct dimeric complexes, XY and XZ.

followed by binding of a second mature protein to form a ternary complex (Fig. 3A, Right). In a “piggy-back” mechanism, a single mature protein binds the nascent peptide while bearing a second mature protein (Fig. 3B). Finally, two mature proteins can bind the same or nearby sites on the nascent peptide—each preventing the other from binding—thereby forming two distinct dimeric complexes, possibly acting as seeds for different multiprotein complexes (Fig. 3C).

The mechanism by which EPRS1 and MARS1 interact with nascent AIMP3 was explored. Stable HEK293T lines were generated in which EPRS1 (shEPRS1), MARS1 (shMARS1), and AIMP3 (shAIMP3) were individually knocked down using lentivirus (Fig. 4A, Left). C-FLAG-EPRS1 was overexpressed in shMARS1 and shCtrl cells and subjected to RIP with anti-FLAG antibody followed by qRT-PCR with primers for AIMP3. Depletion of MARS1 did not alter EPRS1 binding to nascent AIMP3 (Fig. 4A, Top Right). Similarly, MARS1 binding to nascent AIMP3 was unchanged following KD of EPRS1 (Fig. 4A, Bottom Right). The two-way independent binding results are consistent with either a “serial” interaction, in which EPRS1 and MARS1 interact with AIMP3 separately forming distinct binary complexes, or a “concurrent” interaction, in which EPRS1 and MARS1 interact with AIMP3 at the same time to form a single ternary complex. (Fig. 4B, Top). These results are consistent with structural data in which AIMP3 is centrally located between EPRS1 and MARS1 and has distinct binding interfaces for each protein (Fig. 4B, Bottom) (33). To investigate the role of these interactions in MSC inclusion of the constituents, cell lysates from the KD cells were subjected to gel filtration chromatography. EPRS1 KD induced a significant shift of AIMP3 from high-molecular-weight complexes to an ~200-kDa complex (molecular weight of AIMP3 is ~17 kDa) (Fig. 4C). In contrast, MARS1 KD did not influence AIMP3 MSC inclusion despite their cotranslational interaction. A substantial fraction of MARS1 is present in intermediate fractions even in control cells; however, EPRS1 KD induced a marked increase in the extra-MSC fraction. AIMP3 KD did not influence MSC inclusion of either EPRS1 or MARS1. An immunofluorescence experiment

revealed EPRS1 KD induced substantial relocalization of AIMP3 from the cytoplasm to nucleus (Fig. 4D). Interestingly, MARS1-dependent nuclear localization of AIMP3 following DNA damage has been reported (30, 46). Our data suggest EPRS1 does not require interaction with its cotranslational binding partners to incorporate into the MSC; however, both MARS1 and AIMP3 are partially dependent on EPRS1 for MSC inclusion.

IARS1 “Piggybacks” onto LARS1 during Cotranslation with AIMP1.

Remarkably, five MSC constituents interact cotranslationally with nascent AIMP1 (Fig. 1B). The cotranslational interaction of IARS1 and LARS1 with nascent AIMP1 was probed in detail (Fig. 1B, superscript d). Stable lentivirus-driven KD lines were made in HEK293T cells and verified by immunoblot (Fig. 5A, Left). A C-FLAG-IARS1 cDNA construct was transfected into stable shLARS1 cells. Following IP with FLAG antibody, bound AIMP1 mRNA was determined by qRT-PCR. LARS1 KD markedly inhibited binding of IARS1 to nascent AIMP1, revealing a requirement of LARS1 for IARS1–AIMP1 interaction (Fig. 5A, Top Right). In a converse RIP experiment, the interaction of LARS1 with nascent AIMP1 was determined in shIARS1 cells. Following IARS1 KD, the robust interaction of LARS1 with nascent AIMP1 was not significantly diminished (Fig. 5A, Bottom Right). These results are consistent with a “piggyback” mechanism in which IARS1 is carried by LARS1, which interacts directly with nascent AIMP1 (Fig. 5B, Top). To date there is no evidence that LARS1 or IARS1 directly binds AIMP1, but a low-resolution, structural model of the holo-MSC indicates both IARS1 and LARS1 are near the N terminus of AIMP1 (Fig. 5B, Bottom Right). The consequence of perturbation of the IARS1–LARS1–AIMP1 subcomplex was investigated. Cell-free lysates of shCtrl, shIARS1, shLARS1, and shAIMP1 cells were subjected to size-exclusion chromatography. Unexpectedly, IARS1 KD resulted in exclusion of both LARS1 and AIMP1 from the MSC (Fig. 5C); in contrast, LARS1 and AIMP1 KD had no effect on inclusion of either IARS1 or LARS1. These experiments indicate that IARS1 likely influences the retention of LARS1 and AIMP1 within MSC by cotranslational-independent interactions. Despite AIMP1 release

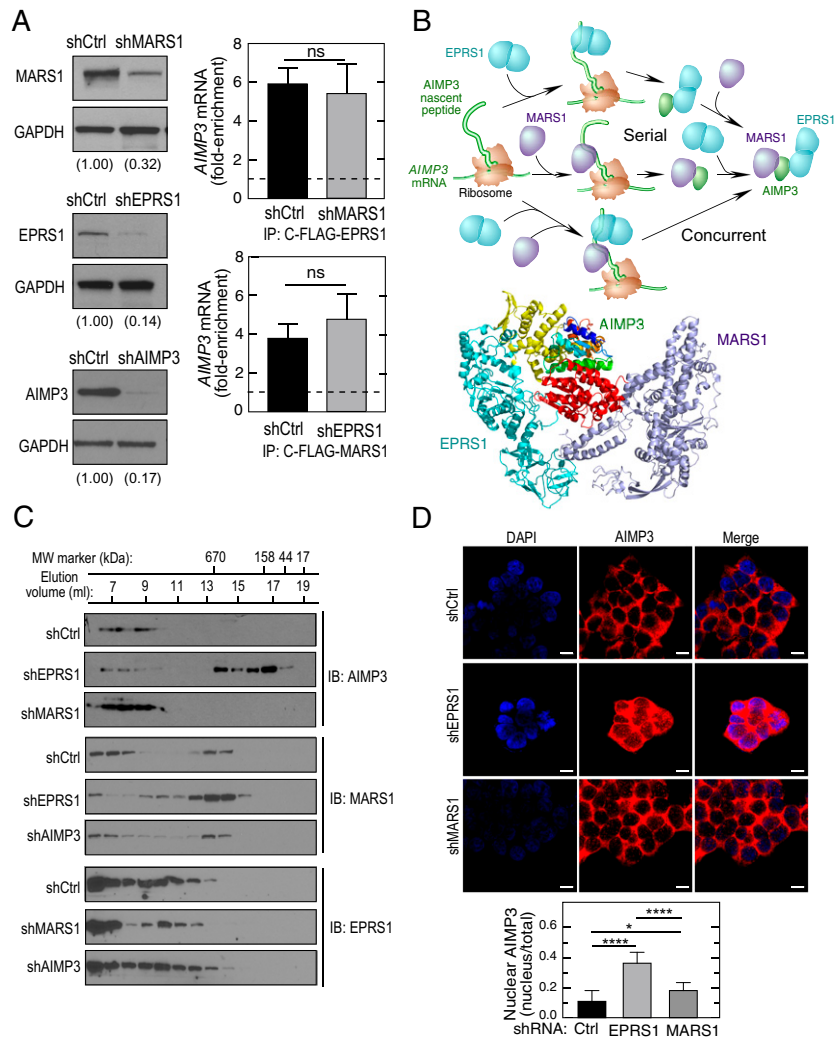


Fig. 4. EPRS1 and MARS1 simultaneously bind AIMP3 cotranslationally. (A) EPRS1 and MARS1 cotranslate with AIMP3 independently. shCtrl and shMARS1 cells were subjected to immunoblot with anti-MARS1 and anti-GAPDH antibodies (*Top Left*). shCtrl and shEPRS1 cells were subjected to immunoblot with anti-EPRS1 and anti-GAPDH antibodies (*Center Left*). shCtrl and shAIMP3 cells were subjected to immunoblot with anti-AIMP3 and anti-GAPDH antibodies (*Bottom Left*). shCtrl and shMARS1 HEK293T cells were transfected with C-FLAG-EPRS1 construct, and lysates subjected to RIP with IgG or anti-FLAG antibodies followed by qRT-PCR with AIMP3 mRNA probe. mRNA is expressed as fold enrichment compared to isotype-specific IgG RIP-qRT-PCR (*Top Right*). shCtrl and shEPRS1 HEK293T cells were transfected with C-FLAG-MARS1 construct and lysates were subjected to RIP with IgG or anti-FLAG antibodies followed by qRT-PCR with AIMP3 mRNA probe (*Bottom Right*). mRNA is expressed as fold enrichment compared to isotype-specific IgG RIP-qRT-PCR. Mean + SD, $n = 3$; ns = nonsignificant. (B) Schematic of alternative, multisite cotranslation pathways between EPRS1, MARS1, and AIMP3 (*Top*). Structure of the GST-like domains of EPRS1–AIMP3–MARS1. (C) EPRS1 influences inclusion of AIMP3 and MARS1 in the MSC. shCtrl, shEPRS1, and shMARS1 cells were subjected to gel filtration chromatography followed by immunoblot with anti-AIMP3, -EPRS1, and -MARS1 antibodies. (D) Immunofluorescence analysis of shCtrl, shEPRS1, and shMARS1 cells using anti-AIMP3 antibody and DAPI (*Top*). (Scale bars, 10 μ m.) Bar plots report the nuclear enrichment of AIMP3; mean + SD, * $P < 0.05$, **** $P < 0.001$ (*Bottom*).

from the MSC in shIARS cells, no change in intracellular localization was observed by immunofluorescence (Fig. 5D).

Discussion

Out of the matrix of 121 cotranslational interactions between human MSC constituents, 15 were observed experimentally. Three MSC constituents have been reported as dimers, i.e., KARS1, EPRS1, and DARS1 (36, 47, 48); however, their homomeric cotranslational interactions were not detected. Unexpectedly, only AIMP3 exhibited homomeric cotranslation. Despite being the smallest protein component of the MSC (~17 kDa), AIMP3 harbors two protein-binding surfaces including the GST-like domain that links four “hub” constituents. AIMP3 dimers have been observed *in vitro* in crystal structures and by the yeast two-hybrid assay (49, 50), but evidence for AIMP3 dimers in the MSC is lacking. Possibly, dimeric AIMP3 performs

an extra-MSC function. Alternatively, AIMP3 self-cotranslation might represent a nonproductive “dead end.” An unexpected finding was the propensity for multiple mature proteins to bind a single nascent peptide; in fact, the majority of the cotranslational interactions observed are in this category. The finding that 13/15 cotranslational interactions involved the three AIMP3s is consistent with the widely accepted concept that they serve as important scaffolding proteins, but our data suggest they have a critical role in MSC assembly as well. The observation that five proteins cotranslationally bind nascent AIMP1 is remarkable and suggests the protein has a particularly critical function in coordinating assembly of the complex. Also noteworthy is the cotranslational interactions of three subcomplexes, i.e., KARS1–AIMP2, EPRS1–AIMP3–MARS1, and IARS1–LARS1, with AIMP1 (Fig. 6). The former two subcomplexes themselves form cotranslationally. Finally, QARS1 cotranslationally interacts with AIMP1. Thus, according to our model, 9/11 MSC constituents cotranslationally

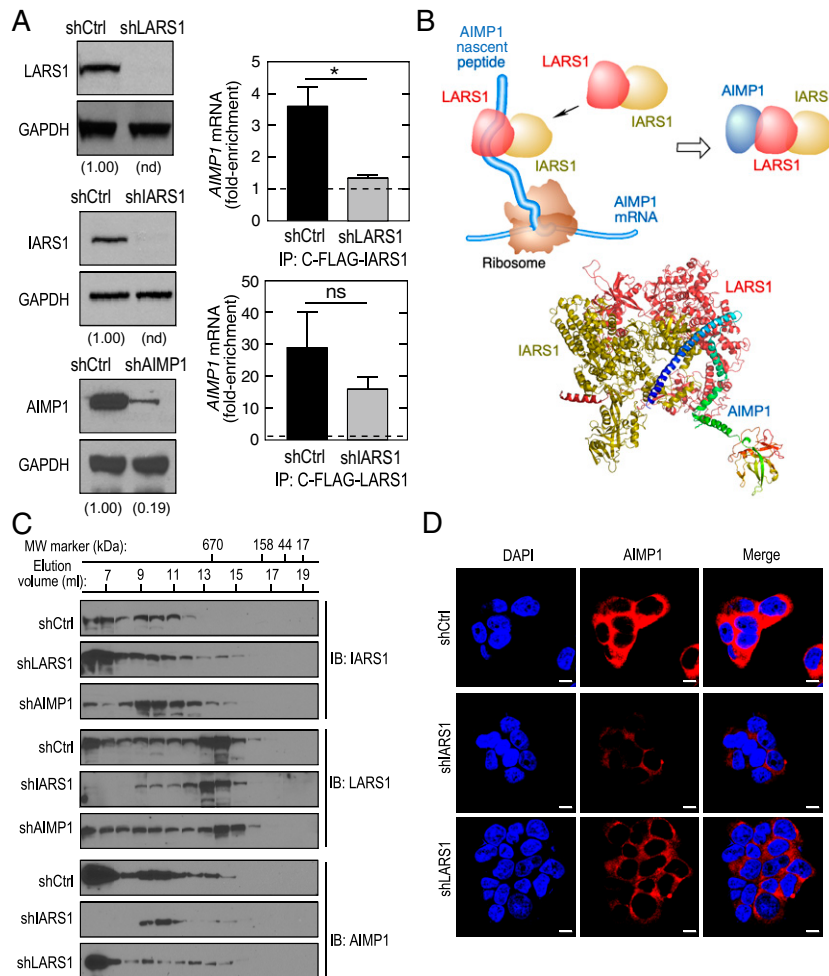


Fig. 5. Piggy-back cotranslation of LARS1 and IARS1 with AIMP1. (A) shCtrl and shLARS1 cells were subjected to immunoblot with anti-LARS1 and anti-GAPDH antibodies (Top Left). shCtrl and shIARS1 cells were subjected to immunoblot with anti-IARS1 and anti-GAPDH antibodies (Center Left). shCtrl and shAIMP1 cells were subjected to immunoblot with anti-AIMP1 and anti-GAPDH antibodies (Bottom Left). shCtrl and shLARS1 HEK293T cells were transfected with C-FLAG-IARS1 construct and lysates subjected to RIP with IgG or anti-FLAG antibodies, followed by qRT-PCR with *AIMP1* mRNA probe (Top Right). mRNA is expressed as fold enrichment compared to isotype-specific IgG RIP-qRT-PCR. Mean + SD, $n = 3$; $*P < 0.05$; ns = nonsignificant. shCtrl and shIARS1 HEK293T cells were transfected with C-FLAG-LARS1 construct and lysates were subjected to RIP with IgG or anti-FLAG antibodies, followed by qRT-PCR with *AIMP1* mRNA probe (Bottom Right). mRNA is expressed as fold enrichment compared to isotype-specific IgG RIP-qRT-PCR. Mean + SD, $n = 3$; ns = nonsignificant. (B) Schematic of piggy-back cotranslation of IARS1 and LARS1 with AIMP1 (Top). Structure of IARS1-LARS1-AIMP1 as determined by XL-MS (Bottom). (C) IARS1 determines inclusion of LARS1 and AIMP3 in the MSC. shCtrl, shLARS1, shIARS1, and shAIMP1 cells were subjected to gel filtration chromatography followed by immunoblot with anti-IARS1, anti-LARS1, and anti-AIMP1 antibodies. (D) Immunofluorescence analysis of shCtrl, shIARS1, and shLARS1 cells using anti-AIMP1 antibody and DAPI. (Scale bars, 10 μ m.)

interact, either directly or indirectly, with AIMP1. Only two constituents are not assembled cotranslationally, namely DARS1 and RARS1. The proposed central role of AIMP1 in MSC assembly is consistent with a recent three-dimensional model of the MSC in which AIMP1 forms a “belt-like” structure encircling much of the MSC (40).

Several cotranslational interactions described here are supported by previous biochemical and X-ray crystallographic data. The cotranslational interaction of mature KARS1 with nascent AIMP2 is consistent with the reported crystal structure and with XL-MS data showing KARS1 binds the N terminus of AIMP2 (36, 40, 51). The role of the AIMP2 N terminus was confirmed by showing that a 36-amino-acid peptide corresponding to this region markedly inhibited cotranslational interaction. shRNA-mediated AIMP2 KD resulted in exclusion of KARS1 from the MSC as shown by gel filtration chromatography. Ser²⁰⁷ phosphorylation of KARS1 alters its structure, reducing its affinity for AIMP2, and induces its release from MSC (28), indicating the critical role of AIMP2 in KARS1 MSC inclusion. Although our data indicate the centrality of AIMP1, not AIMP2, in MSC assembly, studies

in *AIMP2*^{-/-} mice show the essentiality of the latter in MSC stability and mouse viability (52). Cotranslation targeting the N terminus of an emerging peptide to form a protein complex, as observed here, presents multiple advantages. A nascent, unfolded peptide can provide recognition sites that are masked in the mature, folded protein (13). Also, the frequent presence of a “translational ramp” in which rare codons in the first ~50 N-terminal codons hinders translation and might facilitate protein folding (53). Likewise, slow translation near the N terminus can provide a kinetically favorable condition for cotranslation.

The mammalian MSC contains a central “hub” of four proteins that interact via their GST-like domains: AIMP2–EPRS1–AIMP3–MARS1. Multisite cotranslational binding of EPRS1 and MARS1 to nascent AIMP3 is consistent with their established binding partners—AIMP3 is sandwiched between MARS1 and EPRS1 with no direct interaction with AIMP2 (33). Interestingly, the crystal structure shows that MARS1 and EPRS1 bind AIMP3 at distinct, opposing domains, consistent with the observed multisite cotranslational binding. The absence of cotranslational interaction of AIMP2 with either AIMP3 or

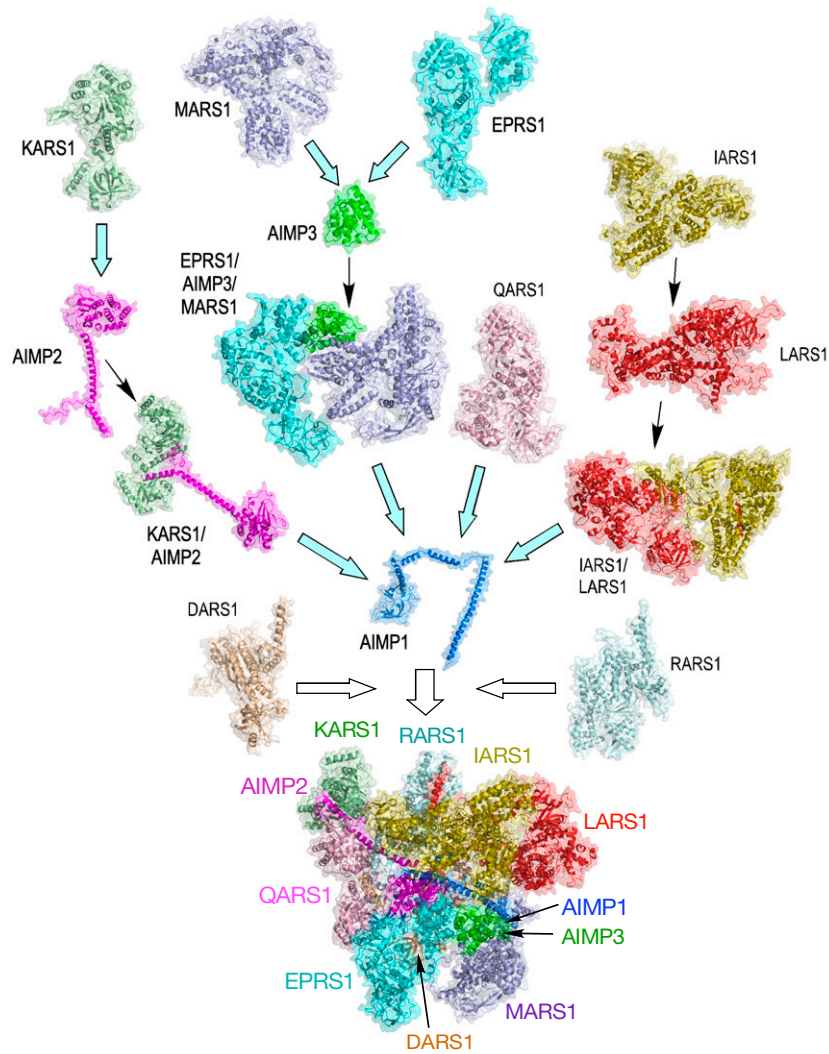


Fig. 6. Schematic of multimodal, cotranslational assembly of the human MSC. Subcomplexes formed by cotranslational (open blue arrows) or posttranslational (open black arrows) interactions coordinate assembly of mature holo-complex.

MARS1, but with EPRS1, further corroborates the crystal structure where AIMP2 physically interacts only with EPRS1 (33). The homologs of these proteins in yeast also assemble cotranslationally (11). Interestingly, each pair of yeast proteins exhibit bidirectional cotranslation; for example, mature EARS1 binds nascent Arc1p, and mature Arc1p binds nascent EARS1. Likewise, a subgroup of the homologs in the mammalian MSC interact cotranslationally—in addition to EPRS1 and MARS1 binding nascent AIMP3, AIMP3 interacts cotranslationally with EPRS1 and MARS1 (Fig. 1*B*, superscript e). In contrast to the yeast MSC, EPRS1 and MARS1 do not interact cotranslationally, an expected result given that the crystal structure does not reveal any interaction (33). The species-specific cotranslational interaction of MARS1 and EARS1 in *Saccharomyces cerevisiae* is noteworthy because complexes of these components have not been reported. Possibly, it is simply a case of a weak, nonproductive interaction due to incidental complementary binding surfaces. Alternatively, the transient interaction might provide a function required during assembly but not in the mature complex. For example, the interaction could mask cryptic organelle-targeting sequences or prevent posttranslational modification that could drive mislocalization and inappropriate or injurious noncanonical function.

A binary interaction between IARS1 and LARS1 has been reported (39, 43), but a subcomplex formed with AIMP1 has

not been reported. A recent *in vitro* investigation of MSC assembly likewise showed this interaction and also showed IARS1 was essential for LARS1 incorporation into the reconstituted MSC (54). The mutual requirement for both supports our observation, but the direct binding protein in that case is IARS1, versus LARS1 in our investigation. There are several possible explanations of this apparent discrepancy. In our experiments we determine the specific requirement for interaction with AIMP1, whereas the reconstitution experiment determined the interactions with an *in vitro*-reconstituted holo-MSC. Moreover, the *in vitro* experiments interrogate interactions between full-length recombinant proteins whereas cotranslation studies determine interactions between mature and nascent endogenous proteins. Surprisingly, shRNA-mediated KD of IARS1 induced substantial depletion of both LARS1 and AIMP1 from the MSC, further supporting the important role of the LARS1–IARS1 complex in MSC structure but also suggesting that the pathway of assembly does not necessarily dictate the pathway of release which depends on an ensemble of interactions. For example, although IARS1 does not directly interact with the N terminus of AIMP1 during assembly of the subcomplex, its subsequent interaction with mature AIMP1 in the holo-complex might be essential for its MSC residence.

These experiments provide compelling evidence that cotranslational interactions contribute to assembly of the human

MSC. Our findings of mechanisms of cotranslation to form multiprotein subcomplexes, i.e., multisite and piggy-back interactions, potentially provide specific, efficient, and temporally ordered assembly pathways. Fig. 6 illustrates a plausible mechanism of assembly driven by independent formation of several subcomplexes by parallel, cotranslational interactions. This pathway is almost certainly oversimplified, as other pathways consistent with the data are possible. For example, the KARS1–AIMP2 complex is shown to cotranslate with nascent AIMP1. However, AIMP2 also cotranslates with nascent AIMP3, and thus an alternative, larger subcomplex might form that cotranslates with AIMP1. Many other important questions remain. For example, we show that a PEM can block the cotranslational interaction between a pair of MSC constituents. However, our results do not address the essentiality of cotranslational interactions for assembly of the holo-MSC. Also, cotranslational assembly raises important questions regarding stimulus-inducible release of specific components from the MSC, generally to perform noncanonical functions unrelated to protein synthesis (24, 26–30). Namely, what is the fate of the fractional MSC and the free constituents? Can released (or de novo generated) constituents reengage the complex without cotranslation? Several groups have speculated on the equilibrium state of the MSC, but experimental evidence is lacking to date (26, 55). Reconstitution of the human MSC from purified, recombinant proteins has been reported (54), but it is not known whether in vitro reconstitution generates a complex that resembles the endogenous MSC—either structurally or functionally. Finally, to date there is no information on the existence of processes that identify misassembled structures and correct them, for example by disassembly, or by targeted degradation. Overall, the finding of a plethora of multimodal cotranslational interactions in MSC assembly represents an informative paradigm for assembly of large, heteromultimeric mammalian complexes.

Materials and Methods

Cell culture, Reagents, Constructs, and Antibodies. HEK293T was purchased from ATCC. The cells were grown in Dulbecco's modified Eagle's medium supplemented with 10% fetal bovine serum and 1% penicillin-streptomycin solution, in a humidified 5% CO₂ chamber. Rabbit anti-MARS1, rabbit anti-AIMP1, rabbit anti-AIMP2, rabbit anti-AIMP3, rabbit anti-KARS1, rabbit anti-IARS1, rabbit anti-LARS1, and rabbit anti-GAPDH antibodies were from Proteintech. Rabbit anti-EPRS1 antibody was generated against the human EPRS1 linker region (Leu₇₅₃-Thr₉₅₆) (BioSynthesis). Normal mouse IgG for isotype control was purchased from Santa Cruz. Goat anti-rabbit antibodies and ECL and ECL prime reagents were obtained from GE Healthcare. Alexa 568 goat anti-rabbit secondary antibodies were from Invitrogen. Lipofectamine 2000 transfection reagent, qPCR probes, Halt Protease Inhibitor mixture, RNase out, DNaseI, glycogen, bicinchoninic acid (BCA) protein estimation kit, and One-step Taqman reaction mix were from Thermo Fisher. LipoD293 transfection reagent was purchased from Signagen. Custom Taqman probes against AIMP1 and primers for mutants were from IDT Technologies. Amicon Ultra4 concentration tubes were from Millipore-Sigma. Mouse anti-FLAG M2 antibody, Cellytic buffer and shRNAs specific for EPRS1, MARS1, AIMP3, KARS1, AIMP2, IARS1, LARS1, and AIMP1 were purchased from Sigma-Aldrich. Puromycin was obtained from Invivogen. cDNA open reading frames expressing C-FLAG EPRS1 were from Genscript, and C-FLAG MARS1, C-FLAG IARS1, C-FLAG LARS1, C-FLAG RARS1, C-FLAG QARS1, C-FLAG DARS1, C-FLAG AIMP1, C-FLAG AIMP2, C-FLAG AIMP3, and C-His AIMP1 were from Sino Biological. DAPI-containing mounting media was from Vector Laboratories and chambered culture slides were from BD.

Lentivirus Production and shRNA-Mediated Gene KD. Recombinant Lenti-Ctrl, Lenti-EPRS1, Lenti-MARS1, Lenti-KARS1, Lenti-IARS1, Lenti-LARS1, Lenti-AIMP1, Lenti-AIMP2, and Lenti-AIMP3 viruses were produced as described (56). Briefly, 2.5×10^5 HEK293T cells were separately transduced with above-described shRNA lentiviral particles in the presence of polybrene (2 µg/mL, vol/vol), and incubated

for 3 d. The cell culture media was replaced with fresh medium containing puromycin (1 µg/mL). Fresh puromycin-containing media was added every 3 d for 3 to 4 wk to select stably knock down cells. KDs were validated by Western blot and cells stored in liquid nitrogen.

Western Blot Analysis. Cells were scraped and washed with ice-cold phosphate-buffered saline (PBS). The pellet was resuspended in Cellytic lysis reagent for 15 m at 4 °C in the presence of 1× protease inhibitor mixture (vol/vol) and debris was removed by centrifugation at 15,000 rpm for 15 m at 4 °C. Samples were quantified by the BCA method; equal protein amounts were subjected to sodium dodecyl sulfate polyacrylamide gel electrophoresis (SDS-PAGE) and transferred by electrophoresis to a poly(vinylidene difluoride) membrane for 45 m at 250 mA. The membrane was blocked with 5% powdered nonfat milk (wt/vol) in Tris-buffered saline containing 0.05% (vol/vol) Tween 20 (TBST) for 1 h at room temperature and then incubated overnight at 4 °C with target-specific primary antibodies. Following three washes with TBST, membranes were incubated with horseradish peroxidase-conjugated secondary antibody for 1 h at room temperature. The blots were washed and developed using ECL reagents per the manufacturer's recommendation.

RIP and qRT-PCR. HEK293T cells were grown to ~80% confluence and transfected with aaRS constructs expressing C-FLAG-tagged proteins (10 µg for single overexpression and 5 µg of each plasmids for coexpression). Briefly, 150-cm plates were treated with either water or puromycin (50 µg/mL) and incubated at 37 °C for 30 m. Following washing with ice-cold PBS, the cells were pelleted and lysed in polysome lysis buffer (100 mM KCl, 5 mM MgCl₂, 10 mM Hepes, pH 7.0, 0.5% Nonidet P-40 [vol/vol], 1 mM dithiothreitol, and 100 units/mL of RNase Out) for 45 m and centrifuged at 15,000 rpm for 15 m. The cleared, cell-free extracts were further precleared using Protein A/G magnetic beads for 1 h at 4 °C in an end-to-end rotator and the beads removed by a magnetic rack. For immunoprecipitations, FLAG antibodies (1:100) were added with 20 µL of pre-equilibrated beads and the mixture was kept overnight at 4 °C with end-to-end mixing. An equal amount of IgG (1:25) was used in control experiments. The beads were washed four times in NT2 buffer (50 mM Tris-HCl, pH 7.4, 150 mM NaCl, 1 mM MgCl₂, and 0.05% Nonidet P-40 [vol/vol]) followed by resuspension in TRIzol for RNA extraction. qPCR was performed with isolated RNA using Taqman probes specific for MSC constituents, and fold enrichment compared to IgG was determined.

Size-Exclusion Chromatography. Cells (3×10^7) were seeded on a 150-cm plate and grown for 24 h until ~90% confluence. The cells were washed in ice-cold PBS twice and pelleted at $1,000 \times g$ for 5 m at 4 °C. The cells were lysed in lysis buffer (100 mM Tris-HCl pH 7.5, 150 mM NaCl, and 1% Triton X-100 [vol/vol]) supplemented with protease inhibitor mixture for 20 m, and the lysates centrifuged to clear debris at $12,000 \times g$ for 15 m. The lysates were further subjected to ultracentrifugation at $100,000 \times g$ for 1 h and protein concentration was determined. Approximately 2.5 mg protein lysate was injected onto a Superose 6 column (30 cm length, 24 mL bed volume) pre-equilibrated with mass spectrometry running buffer (20 mM Tris-HCl, pH 7.5, and 150 mM NaCl). Thirty fractions of 500 µL were collected and an equal volume of alternate fractions was analyzed by SDS-PAGE and western blotting.

Confocal Microscopy. Two-chamber BD culture slides were seeded with cells (5×10^3 cells per chamber) allowed to adhere for 24 h. Cells were rinsed carefully with ice-cold PBS and fixed with 1:1 solution of methanol and acetone for 30 m at –20 °C. The slides were air-dried for 15 m and rehydrated in PBS for 15 m. The slides were blocked with PBS containing 3% goat serum for 1 h at room temperature. Antibodies against AIMP1, AIMP3, and KARS1 (all 1:500) diluted in blocking buffer were incubated with the slides overnight at 4 °C. The slides were washed with ice-cold PBS containing 1% Tween 20 three times for 5 m and incubated with Alexa 568-labeled anti-rabbit secondary antibody (1:500, vol/vol) diluted in blocking buffer at room temperature for 1 h. Following three more washes as above, vectashield containing DAPI was used to mount cells. Images were acquired at 63×/1.40 numerical aperture with a Leica TCS-SP8-AOBS inverted confocal microscope (Leica Microsystems, GmbH). The quantification was done using Image-Pro Plus 7 (Media Cybernetics) using 10 cells for each condition.

Cell Treatments. For treatments with peptides, HEK293T cells were transfected with a C-FLAG-KARS1 construct overnight. Then cells were incubated with 100 μ M of AIMP2 and scrambled Arg₉-peptides. Peptides sequences: ARG₉-AIMP2, RRRRRRRRMPMYQVKPYHGGGAPLRVLPCTCMYRLPNVHGSRYSYG; ARG₉-scrambled: RRRRRRRRYPMLAPGVMMRPYVEHYGLHVQTPCGPYSRGRKNG. After 6 h, the cells were harvested and RIP-qRT-PCR experiments done as described above.

Molecular Modeling. Structural models of individual constituents and subcomplexes of the MSC and the holo-MSC were generated from reported structures and extended and modified by XL-MS as described previously (40, 41).

Statistical Analysis. Each experiment was performed in triplicate unless otherwise described. The data are expressed as the mean + SD. Statistical analysis was done by Student's *t* test using Prism 7.0 (GraphPad), and *P* < 0.05 was considered statistically significant.

1. N. J. Krogan *et al.*, Global landscape of protein complexes in the yeast *Saccharomyces cerevisiae*. *Nature* **440**, 637–643 (2006).
2. P. C. Havgugimana *et al.*, A census of human soluble protein complexes. *Cell* **150**, 1068–1081 (2012).
3. J. A. Marsh, S. A. Teichmann, Structure, dynamics, assembly, and evolution of protein complexes. *Annu. Rev. Biochem.* **84**, 551–575 (2015).
4. A. Schweitzer *et al.*, Structure of the human 26S proteasome at a resolution of 3.9 Å. *Proc. Natl. Acad. Sci. U.S.A.* **113**, 7816–7821 (2016).
5. M. Selmer *et al.*, Structure of the 70S ribosome complexed with mRNA and tRNA. *Science* **313**, 1935–1942 (2006).
6. B. L. Wagner, A. Bauer, G. Schütz, M. Montminy, Stimulus-specific interaction between activator-coactivator cognates revealed with a novel complex-specific antiserum. *J. Biol. Chem.* **275**, 8263–8266 (2000).
7. J. Zhao *et al.*, Multifaceted stoichiometry control of bacterial operons revealed by deep proteome quantification. *Front. Genet.* **10**, 473 (2019).
8. J. N. Wells, L. T. Bergendahl, J. A. Marsh, Operon gene order is optimized for ordered protein complex assembly. *Cell Rep.* **14**, 679–685 (2016).
9. A. Halbach *et al.*, Cotranslational assembly of the yeast SET1C histone methyltransferase complex. *EMBO J.* **28**, 2959–2970 (2009).
10. C. D. Duncan, J. Mata, Widespread cotranslational formation of protein complexes. *PLoS Genet.* **7**, e1002398 (2011).
11. A. Shiber *et al.*, Cotranslational assembly of protein complexes in eukaryotes revealed by ribosome profiling. *Nature* **561**, 268–272 (2018).
12. I. Kamenova *et al.*, Co-translational assembly of mammalian nuclear multisubunit complexes. *Nat. Commun.* **10**, 1740 (2019).
13. K. Khan *et al.*, Cotranslational interaction of human EBP50 and ezrin overcomes masked binding site during complex assembly. *Proc. Natl. Acad. Sci. U.S.A.* **119**, e2115799119 (2022).
14. J. Lu, J. M. Robinson, D. Edwards, C. Deutsch, T1-T1 interactions occur in ER membranes while nascent Kv peptides are still attached to ribosomes. *Biochemistry* **40**, 10934–10946 (2001).
15. M. Ibba, D. Söll, Aminoacyl-tRNAs: Setting the limits of the genetic code. *Genes Dev.* **18**, 731–738 (2004).
16. S. Havrylenko, M. Mirande, Aminoacyl-tRNA synthetase complexes in evolution. *Int. J. Mol. Sci.* **16**, 6571–6594 (2015).
17. H. Simader *et al.*, Structural basis of yeast aminoacyl-tRNA synthetase complex formation revealed by crystal structures of two binary sub-complexes. *Nucleic Acids Res.* **34**, 3968–3979 (2006).
18. L. Guigou, V. Shalakh, M. Mirande, The tRNA-interacting factor p43 associates with mammalian arginyl-tRNA synthetase but does not modify its tRNA aminoacylation properties. *Biochemistry* **43**, 4592–4600 (2004).
19. E. Barbarese *et al.*, Protein translation components are colocalized in granules in oligodendrocytes. *J. Cell Sci.* **108**, 2781–2790 (1995).
20. B. S. Negrutskii, M. P. Deutscher, Channeling of aminoacyl-tRNA for protein synthesis *in vivo*. *Proc. Natl. Acad. Sci. U.S.A.* **88**, 4991–4995 (1991).
21. M. Kaminska *et al.*, Dynamic organization of aminoacyl-tRNA synthetase complexes in the cytoplasm of human cells. *J. Biol. Chem.* **284**, 13746–13754 (2009).
22. A. David *et al.*, RNA binding targets aminoacyl-tRNA synthetases to translating ribosomes. *J. Biol. Chem.* **286**, 20688–20700 (2011).
23. N. Netzer *et al.*, Innate immune and chemically triggered oxidative stress modifies translational fidelity. *Nature* **462**, 522–526 (2009).
24. P. Sampath *et al.*, Noncanonical function of glutamyl-prolyl-tRNA synthetase: Gene-specific silencing of translation. *Cell* **119**, 195–208 (2004).
25. H. Cui *et al.*, Regulation of ex-translational activities is the primary function of the multi-tRNA synthetase complex. *Nucleic Acids Res.* **49**, 3603–3616 (2021).
26. P. S. Ray, A. Arif, P. L. Fox, Macromolecular complexes as depots for releasable regulatory proteins. *Trends Biochem. Sci.* **32**, 158–164 (2007).
27. A. Arif *et al.*, EPRS is a critical mTORC1-S6K1 effector that influences adiposity in mice. *Nature* **542**, 357–361 (2017).
28. Y. Ofir-Birin *et al.*, Structural switch of lysyl-tRNA synthetase between translation and transcription. *Mol. Cell* **49**, 30–42 (2013).
29. Y. G. Ko, Y. S. Kang, E. K. Kim, S. G. Park, S. Kim, Nucleolar localization of human methionyl-tRNA synthetase and its role in ribosomal RNA synthesis. *J. Cell Biol.* **149**, 567–574 (2000).

Data, Materials, and Software Availability. All study data are included in the article and/or supporting information.

ACKNOWLEDGMENTS. Research was supported by National Institute of Diabetes and Digestive and Kidney Diseases (R01 DK124203 and R01 DK123236 to P.L.F.), National Institute on Aging (R01 AG067146 to P.L.F.), National Institute of Neurological Disorders and Stroke (R01 NS124547 to P.L.F. and V.G.), Research Accelerator Program Grant from the Lerner Research Institute, Cleveland Clinic (to P.L.F.), and VelaSano 6 Pilot Award (to P.L.F.).

Author affiliations: ^aDepartment of Cardiovascular and Metabolic Sciences, Lerner Research Institute, Cleveland Clinic, Cleveland, OH 44195; ^bDepartment of Chemistry, Cleveland State University, Cleveland, OH 44115; and ^cImaging Core, Lerner Research Institute, Cleveland Clinic, Cleveland, OH 44195

30. N. H. Kwon *et al.*, Dual role of methionyl-tRNA synthetase in the regulation of translation and tumor suppressor activity of aminoacyl-tRNA synthetase-interacting multifunctional protein-3. *Proc. Natl. Acad. Sci. U.S.A.* **108**, 19635–19640 (2011).
31. A. Arif, J. Jia, R. A. Moodt, P. E. DiCorleto, P. L. Fox, Phosphorylation of glutamyl-prolyl tRNA synthetase by cyclin-dependent kinase 5 dictates transcript-selective translational control. *Proc. Natl. Acad. Sci. U.S.A.* **108**, 1415–1420 (2011).
32. J. M. Han *et al.*, AIMP2/p38, the scaffold for the multi-tRNA synthetase complex, responds to genotoxic stresses via p53. *Proc. Natl. Acad. Sci. U.S.A.* **105**, 11206–11211 (2008).
33. H. Y. Cho *et al.*, Assembly of multi-tRNA synthetase complex via heterotetrameric glutathione transferase-homology domains. *J. Biol. Chem.* **290**, 29313–29328 (2015).
34. H. Y. Cho *et al.*, Symmetric assembly of a decameric subcomplex in human multi-tRNA synthetase complex via interactions between glutathione transferase-homology domains and aspartyl-tRNA synthetase. *J. Mol. Biol.* **431**, 4475–4496 (2019).
35. Y. Fu *et al.*, Structure of the ArgRS-GlnRS-AIMP1 complex and its implications for mammalian translation. *Proc. Natl. Acad. Sci. U.S.A.* **111**, 15084–15089 (2014).
36. Z. Hei, S. Wu, Z. Liu, J. Wang, P. Fang, Retractable lysyl-tRNA synthetase-AIMP2 assembly in the human multi-aminoacyl-tRNA synthetase complex. *J. Biol. Chem.* **294**, 4775–4783 (2019).
37. M. Guo, X. L. Yang, P. Schimmel, New functions of aminoacyl-tRNA synthetases beyond translation. *Nat. Rev. Mol. Cell Biol.* **11**, 668–674 (2010).
38. M. Mirande, Aminoacyl-tRNA synthetase family from prokaryotes and eukaryotes: Structural domains and their implications. *Prog. Nucleic Acid Res. Mol. Biol.* **40**, 95–142 (1991).
39. S. B. Rho *et al.*, Genetic dissection of protein-protein interactions in multi-tRNA synthetase complex. *Proc. Natl. Acad. Sci. U.S.A.* **96**, 4488–4493 (1999).
40. K. Khan, C. Baleanu-Gogonea, B. Willard, V. Gogonea, P. L. Fox, 3-dimensional architecture of the human multi-tRNA synthetase complex. *Nucleic Acids Res.* **48**, 8740–8754 (2020).
41. K. Khan, C. Baleanu-Gogonea, B. Willard, V. Gogonea, P. L. Fox, An optimized protocol for *in vitro* and *in cellulo* structural determination of the multi-tRNA synthetase complex by cross-linking mass spectrometry. *STAR Protoc* **3**, 101201 (2022).
42. V. Albanese, S. Reissmann, J. Frydman, A ribosome-anchored chaperone network that facilitates eukaryotic ribosome biogenesis. *J. Cell Biol.* **189**, 69–81 (2010).
43. J. Kong, S. Kim, Cell-based analysis of pairwise interactions between the components of the multi-tRNA synthetase complex. *FASEB J.* **34**, 10476–10488 (2020).
44. I. Carmi-Levy *et al.*, Importin beta plays an essential role in the regulation of the LysRS-Ap(4A) pathway in immunologically activated mast cells. *Mol. Cell Biol.* **31**, 2111–2121 (2011).
45. R. Halwani *et al.*, Cellular distribution of Lysyl-tRNA synthetase and its interaction with Gag during human immunodeficiency virus type 1 assembly. *J. Virol.* **78**, 7553–7564 (2004).
46. B. J. Park *et al.*, The haploinsufficient tumor suppressor p18 upregulates p53 via interactions with ATM/ATR. *Cell* **120**, 209–221 (2005).
47. H. Zhou, L. Sun, X. L. Yang, P. Schimmel, ATP-directed capture of bioactive herbal-based medicine on human tRNA synthetase. *Nature* **494**, 121–124 (2013).
48. G. Eriani *et al.*, Role of dimerization in yeast aspartyl-tRNA synthetase and importance of the class II invariant proline. *Proc. Natl. Acad. Sci. U.S.A.* **90**, 10816–10820 (1993).
49. K. J. Kim *et al.*, Determination of three-dimensional structure and residues of the novel tumor suppressor AIMP3/p18 required for the interaction with ATM. *J. Biol. Chem.* **283**, 14032–14040 (2008).
50. S. Quevillon, J. C. Robinson, E. Berthonneau, M. Siatecka, M. Mirande, Macromolecular assemblage of aminoacyl-tRNA synthetases: Identification of protein-protein interactions and characterization of a core protein. *J. Mol. Biol.* **285**, 183–195 (1999).
51. A. Rémond *et al.*, Identification of protein interfaces within the multi-aminoacyl-tRNA synthetase complex: The case of lysyl-tRNA synthetase and the scaffold protein p38. *FEBS Open Bio* **6**, 696–706 (2016).
52. J. Y. Kim *et al.*, p38 is essential for the assembly and stability of macromolecular tRNA synthetase complex: Implications for its physiological significance. *Proc. Natl. Acad. Sci. U.S.A.* **99**, 7912–7916 (2002).
53. K. Fredrick, M. Ibba, How the sequence of a gene can tune its translation. *Cell* **141**, 227–229 (2010).
54. R. J. Liu *et al.*, Molecular basis of the multifaceted functions of human leucyl-tRNA synthetase in protein synthesis and beyond. *Nucleic Acids Res.* **48**, 4946–4959 (2020).
55. Y. G. Ko *et al.*, Glutamine-dependent antiapoptotic interaction of human glutamyl-tRNA synthetase with apoptosis signal-regulating kinase 1. *J. Biol. Chem.* **276**, 6030–6036 (2001).
56. K. Khan, B. Long, G. M. Deshpande, P. L. Fox, Bidirectional tumor-promoting activities of macrophage ezrin. *Int. J. Mol. Sci.* **21**, 7716 (2020).